Supporting Information for

Solid-state phase transformation and self-assembly of amorphous nanoparticles into higher-order mineral structures

Stanislas Von Euw[1,7*], Thierry Azaïs[2], Viacheslav Manichev[3,4], Guillaume Laurent[2], Gérard Pehau-Arnaudet[5], Margarita Rivers[4,6], Nagarajan Murali[3], Daniel J. Kelly[7], Paul G. Falkowski[1,3*]

[1]Environmental Biophysics and Molecular Ecology Program, Department of Marine and Coastal Sciences, Rutgers University, 71 Dudley Road, New Brunswick, New Jersey, 08901, United States.

[2]Laboratoire de Chimie de la Matière Condensée de Paris, Sorbonne Université, CNRS, 4 place Jussieu, F-75005, Paris, France.

[3]Department of Chemistry and Chemical Biology, Rutgers University, 123 Bevier Road, Piscataway, New Jersey, 08854, United States.

[4]Institute of Advanced Materials, Devices, and Nanotechnology, Rutgers University, 607 Taylor Road, Piscataway, New Jersey, 08854, United States.

[5]UMR 3528 and UTech UBI, Institut Pasteur, 28 rue du Docteur Roux, F-75015 Paris, France.

[6]Department of Physics, Wellesley College, 106 Central Street, Wellesley, Massachusetts, 02481, United States.

[7]Trinity Centre for Bioengineering, Trinity Biomedical Sciences Institute, Trinity College Dublin, Dublin 2, D02 R590, Ireland.

[*]correspondence to: voneuws@tcd.ie; falko@marine.rutgers.edu

This PDF file includes:

Materials and Methods

Samples preparation procedures. Synthetic, ^{13}C-labeled Amorphous Calcium Magnesium Carbonate (ACMC) was prepared following the protocol described by H. Nebel and M. Epple [1]. The sample was precipitated from two 100 ml solutions: an aqueous solution containing 0.05 M of K_2CO_3 (^{13}C, 98% - Cambridge Isotope Laboratories, Inc.) (pH = 11.4); and an aqueous solution containing 0.045 M of $CaCl_2.2H_2O$ (Sigma-Aldrich) and 0.053 M of $MgCl_2.6H_2O$ (Sigma-Aldrich) (pH = 8.6). The calcium and magnesium-containing solution was poured directly into the carbonate solution. The resulting precipitate was isolated by filtration using a 0.2 µm pore size membrane filter on a vacuum filtration apparatus, washed with anhydrous ethanol, and then, dried at 37°C for a week. A ^{13}C-labeled monohydrocalcite (MHC) sample was prepared following the protocol described by R. Nishiyama et al [2]. It was precipitated from two different solutions: an aqueous solution containing 0.051 M of $CaCl_2$ (Sigma-Aldrich) and 0.010 M of $MgCl_2.6H_2O$ (Sigma-Aldrich) (30 ml); and an aqueous solution containing 0.077 M of Na_2CO_3 (^{13}C, 99% - Sigma-Aldrich) (15 ml). The carbonate solution was poured directly into the calcium and magnesium-containing solution. The resulting mixture was constantly stirred for 24 h to age the precipitate. The precipitate was isolated by centrifugation, washed with deionized water, and then, dried at 37°C for a week. The stony coral sample (*Stylophora pistillata*) was obtained from a nubbin growing in an 800 L custom-designed aquarium at the Department of Marine and Coastal Sciences (DMCS) at Rutgers University. The coral tissue of a skeletal branch belonging to this nubbin was spontaneously dissociated in deionized water for a few hours. The branch was washed under a water jet, dried under air flow at room temperature, transversely sectioned, and slightly etched in an aqueous solution of 1% formic acid for 10 s.

Estimation of the atomic Ca/Mg ratio. The average atomic Ca/Mg ratio of the amorphous calcium magnesium carbonate (ACMC) nanoparticles and that of the ACMC nanoparticles converted into monohydrocalcite following crystallization in the MAS rotor, were estimated using energy-dispersive X-ray spectroscopy (EDS) on a Phenom PROX desktop scanning electron microscope (SEM) operating at 15 kV. The powders were compressed into disks with a smooth surface that were mounted on aluminum studs using carbon adhesive tape. The average atomic Ca/Mg ratio was calculated from 20 random, replicate measurements.

Powder X-ray diffraction (XRD) analysis. The XRD patterns were recorded using a Philips Xpert System X-Ray Diffraction System operating in the reflection mode at CuKα radiation, with 40 kV beam voltage and 40 mA beam current.

Scanning helium ion microscopy (SHIM). SHIM was carried out on a Carl Zeiss Orion Plus Helium Ion Microscope (Carl Zeiss Microscopy, Peabody, MA) operating at 30 kV with a beam current of ≈ 1 pA. An electron flood gun was used for charge neutralization at an accelerating voltage of 900 eV. The vacuum reading in the analysis chamber was $2x10^{-7}$ torr. All the samples were carbon coated prior to SHIM observations.

Cryogenic transmission electron microscopy (cryo-TEM). Cryogenic TEM observations were performed with a Tecnai F20 (Thermo Fisher) operating at 200 kV. The amorphous

powder was first suspended in deionized water in a 10 ml vial (mass concentration, ≈ 2% w/v) and the resulting suspension was sonicated for 2 min. One drop of this suspension was cryofixed immediately after sonication (observations of the amorphous nanoparticles) or after a period of 24 h to allow crystallization (observations of the higher-order mineral structures). To this end, these drops were deposited on glow discharged 300 mesh lacey carbon copper grids that were cryofixed in liquid ethane using a cryo-fixation device (EMGP-Leica). The grids were then transferred inside the microscope using a 626DH cryoholder (Gatan). Images were acquired using a Falcon II direct detector (Thermo Fisher) or a Gatan US 4000 camera (to record the diffraction patterns). Diffraction patterns were acquired in low dose selected area diffraction mode at 1.5 m camera length.

Thermogravimetric analysis coupled with differential scanning calorimetry (TGA/DSC).

Simultaneous TGA/DSC was performed using a Stanton Redcroft STA 1500 (Thorn Scientific). The measurements were performed from room temperature to 1000°C in air atmosphere with a heating rate of 5 °C/min.

Solid-state nuclear magnetic resonance (ssNMR) spectroscopy.

Solid-state NMR spectroscopy experiments were conducted at room temperature on 7.0 T (Fig. 3, Fig. S5, Fig. S6, Fig. S10 and Fig. S11) and 9.4 T (Fig. 2, Fig. 4, Fig. 5, Fig. 6, Fig. S3, Fig. S4, Fig. S7, Fig. S12, Fig. S13 and Fig. S14) AVANCE III Bruker spectrometers operating at $\nu(^1H)$ = 300 and 400 MHz, respectively. The former spectrometer was equipped with a 4 mm Bruker double resonance magic angle spinning (MAS) probe, whereas the latter spectrometer was equipped with a 3.2 mm Bruker E-Free MAS probe. Powdered samples were packed into 3.2 mm or 4.0 mm (o.d.) zirconia MAS rotors and spun at 20 and 14 kHz (dry conditions) or 8 kHz (wet conditions). To carry out the experiments in wet conditions, the powder (about 10-13mg) was first loosely packed into the rotor. The MAS rotor was spun at high frequency for a few minutes so that a vacant space forms at the center of the rotor, and, hence, this vacant space was filled up with deionized water (about 35-38mg) or heavy water (about 39-42mg) and, hence, the rotor for spun at 8 kHz during analysis. Our TGA measurements show that, in dry conditions, the mass fraction of the different populations of hydrogen-bearing ions/molecules (OH^- and H_2O) associated with the particles of ACMC is in the range of 22 to 26 wt. %. As a result, the proportion of hydrogens originating from the particles over the total number of hydrogens (powder soaked in H_2O) or hydrogens + deuteriums (powder soaked in D_2O) present in the MAS rotor following the wetting step can be calculated: i.e., from about 5 to 10%. A one dimensional (1D) ^1H direct excitation (DE) experiments using a composite pulse sequence for an efficient background suppression (i.e. the pulse program from Bruker named zgbs), along with 1D ^{13}C SP (using the high power decoupling pulse program from Bruker named HPDEC), 1D $\{^1H\}^{13}C$ cross polarization (CP), 1D $\{^1H\text{-}^{13}C\}^1H$ double CP, two dimensional (2D) $\{^1H\}^{13}C$ Heteronuclear Correlation (HetCor), and 2D ^{13}C-^{13}C Dipolar Assisted Rotational Resonance (DARR) ssNMR experiments were performed. The recycling delay (RD), number of scans (NS); MAS frequency (ν_{MAS}), and if applicable, contact time (t_{CP}), number of t1 increments and the mixing time (τmix) are all given in the captions of the different Figures. For the 1D ^{13}C SP, 1D $\{^1H\}^{13}C$ CP, 2D $\{^1H\}^{13}C$ HetCor and 2D ^{13}C-^{13}C DARR experiments, ^1H heteronuclear decoupling at a field of 60 kHz (300 MHz spectrometer - Fig. 3; Fig. S10A, and Fig. S11) or

70 kHz (400 MHz spectrometer - Fig. 2, Fig. 4, Fig. 5, Fig. 6, Fig. S3, Fig. S4, Fig. S7, Fig. S12, Fig. S13, and Fig. S14) was applied during acquisition using SPINAL64 heteronuclear decoupling. For the 2D ^{13}C-^{13}C DARR experiments, the States-TPPI method was used for the quadrature detection of the indirect dimension; incremented delay t1 was equal to 3µs; radio frequency (RF) fields (B1) applied during the CP step was $\nu RF(^{1}H)$ = 70 kHz and $\nu RF(^{13}C)$ = 50 kHz with a 90–100% tangential ramp; and a ^{1}H irradiation field of 8 kHz was used during the mixing period of 500 ms to fulfill the rotary resonance conditions (MAS frequency, ν_{MAS} = 8 kHz). For the 2D $\{^{1}H\}^{13}C$ HetCor experiments, the States-TPPI method was used for the quadrature detection of the indirect dimensions; incremented delay t1 was equal to 3µs; and radio frequency (RF) fields (B1) applied during the CP step was $\nu RF(^{1}H)$ = 80 kHz and $\nu RF(^{13}C)$ = 60 kHz (400 MHz spectrometer - Fig. 4, Fig. 5 and Fig. 6), or $\nu RF(^{1}H)$ = 70 kHz and $\nu RF(^{13}C)$ = 50 kHz (300 MHz spectrometer - Fig. S11) with a 90–100% tangential ramp. As for the $\{^{1}H$-$^{13}C\}^{1}H$ double CP experiment, radio frequency (RF) fields (B1) applied during the CP steps was $\nu RF(^{1}H)$ = 70 kHz and $\nu RF(^{13}C)$ = 50 kHz. This experiment consists of two consecutive CP transfers: $^{1}H \rightarrow {}^{13}C$ (during t_{CP1}) followed by $^{13}C \rightarrow {}^{1}H$ (during t_{CP2}). After the first transfer, the ^{13}C magnetization is flipped back to the z direction through a 90° pulse while the ^{1}H residual signal is eliminated by two low power pulses phase shifted by 90° at $\nu RF = \nu MAS/2$ = 7 kHz (HORROR condition). The length of each pulse corresponds to the length of the ^{1}H free induction decay (≈ 10 ms). Following this step, the ^{13}C magnetization is then flipped back into the transverse plane via a 90° pulse and the second CP transfer is then applied prior to ^{1}H acquisition. For all experiments, ^{1}H and ^{13}C chemical shifts were referenced to adamantane at 1.85 ppm and 38.52 ppm (left peak), respectively.

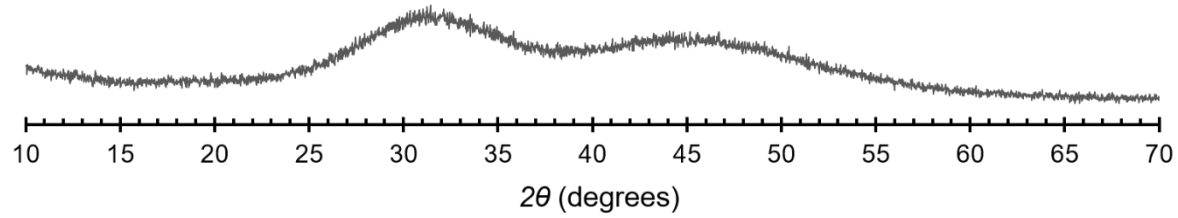

Figure S1. X-ray diffraction analysis of the amorphous powder. Powder X-Ray diffraction pattern of the synthetic, Amorphous Calcium Magnesium Carbonate (ACMC) sample in dry conditions.

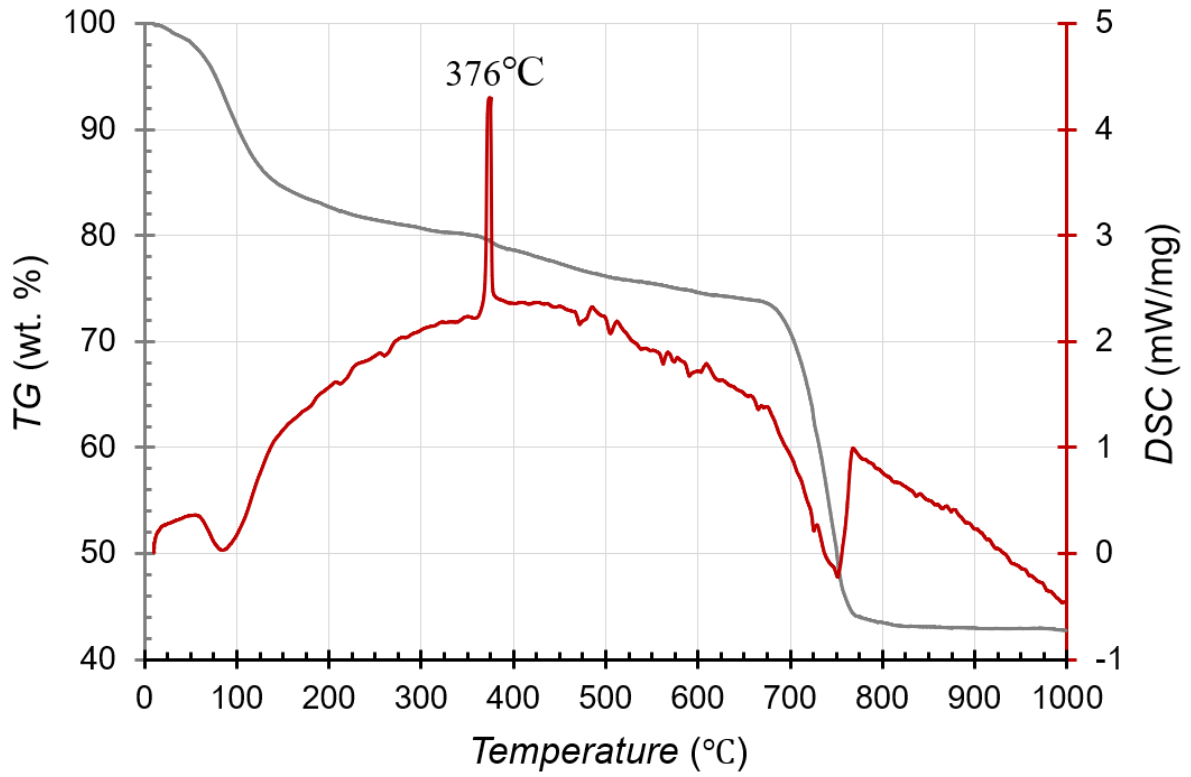

Figure S2. Weight loss and heat flow measurements of the synthetic amorphous nanoparticles. Thermogravimetric analysis (TGA; gray curve) coupled with differential scanning calorimetry (DSC; red curve) of the synthetic, Amorphous Calcium Magnesium Carbonate (ACMC) sample in dry conditions. The TGA curve shows three major mass loss steps visible in the ranges 25 to 150°C, 330 to 420°C and 670 to 780°C. The first and second steps are respectively associated with a broad endotherm and a sharp crystallization exotherm (at 376°C) in the DSC thermogram. These two steps correspond to the removal of different hydrous species [3] associated with a mass loss of about 22%. The latter step is associated with a second broad endotherm in the DSC thermogram and corresponds to the release of $CO_{2(g)}$ following a decarbonation reaction. We also note that the mass fraction of the different hydrous species could be slightly higher than 22% since the mass loss reaches up about 26% before the decarbonation reaction occurs.

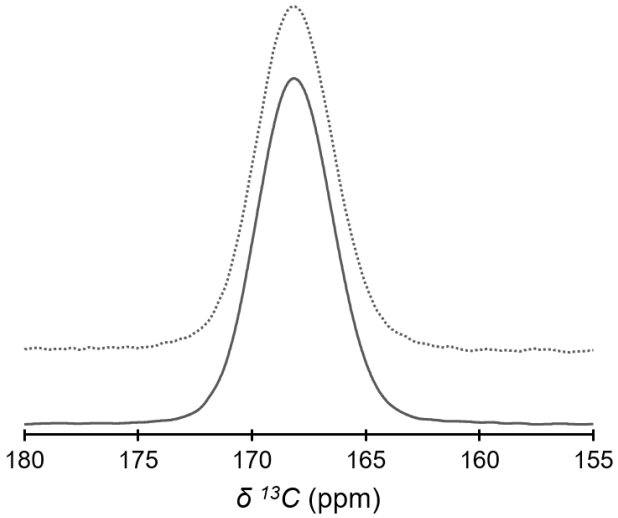

Figure S3. Carbon environments of the synthetic amorphous nanoparticles. ^{13}C-based ssNMR experiments of the synthetic, Amorphous Calcium Magnesium Carbonate (ACMC) sample in dry conditions. Solid lines = normalized 1D {^{1}H}^{13}C cross polarization (CP) MAS ssNMR spectrum (contact time, t_{CP} = 4 ms; number of scans, NS = 400; relaxation delay, RD = 3 s; MAS frequency, ν_{MAS} = 20 kHz); dotted lines = normalized 1D ^{13}C single-pulse (SP) MAS ssNMR spectrum (NS = 8; RD = 600 s; ν_{MAS} = 20 kHz).

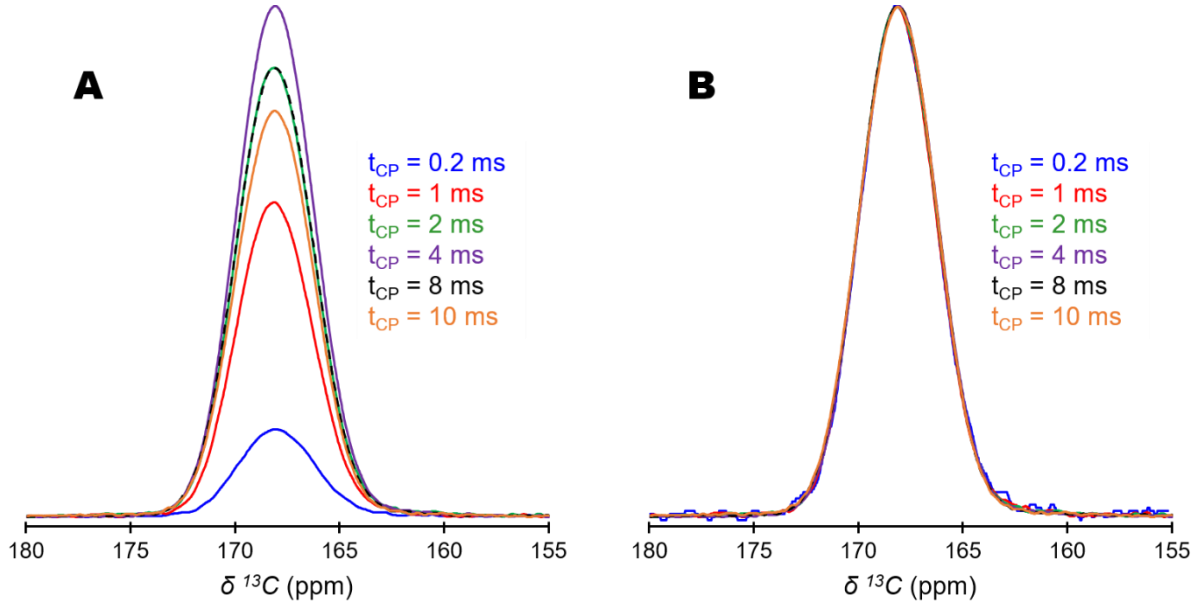

Figure S4. Cross-polarization dynamics between ^{1}H and ^{13}C nuclei in the synthetic amorphous nanoparticles. (**A**) Non-normalized 1D $\{^{1}H\}^{13}C$ cross polarization (CP) MAS ssNMR spectra (contact time, t_{CP} varied from 0.2 to 10ms; number of scans, NS = 400; relaxation delay, RD = 3 s; MAS frequency, ν_{MAS} = 20 kHz) of the synthetic, Amorphous Calcium Magnesium Carbonate (ACMC) sample in dry conditions. (**B**) Normalized 1D $\{^{1}H\}^{13}C$ cross polarization (CP) MAS ssNMR spectra shown in (A). All these spectra expose a single, symmetric resonance whose line shape and line width are constant across the different t_{CP}: $\delta(^{13}C)$ = 168.2 ppm and full width at half maximum (FWHM) = 3.9 ppm. These features are similar with those observed upon direct excitation in the quantitative ^{13}C SP MAS ssNMR spectra of Fig. S3.

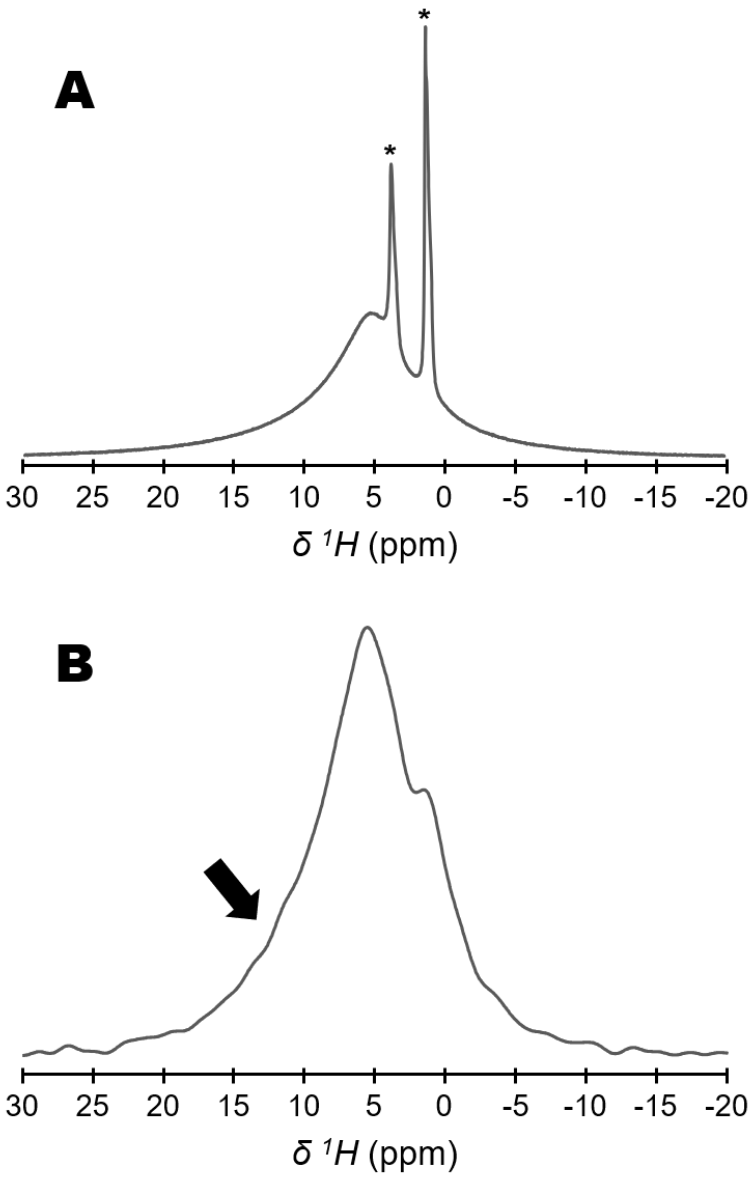

Figure S5. Hydrogen-bearing ions/molecules associated with the amorphous nanoparticles. (A) 1D ^{1}H direct excitation (DE) MAS ssNMR spectrum (number of scans, NS = 32; relaxation delay, RD = 2 s; MAS frequency, ν_{MAS} = 14 kHz) of the synthetic, Amorphous Calcium Magnesium Carbonate (ACMC) sample in dry conditions. The two narrow resonances (*) are due to the presence of ethanol. **(B)** 1D {^{1}H-^{13}C}^{1}H double cross polarization (CP) MAS ssNMR spectrum (number of scans, NS = 640; relaxation delay, RD = 2 s; contact time-1, t_{CP1} = 4 ms; contact time-2, t_{CP2} = 4 ms; ν_{MAS} = 14 kHz) of ACMC in dry conditions.

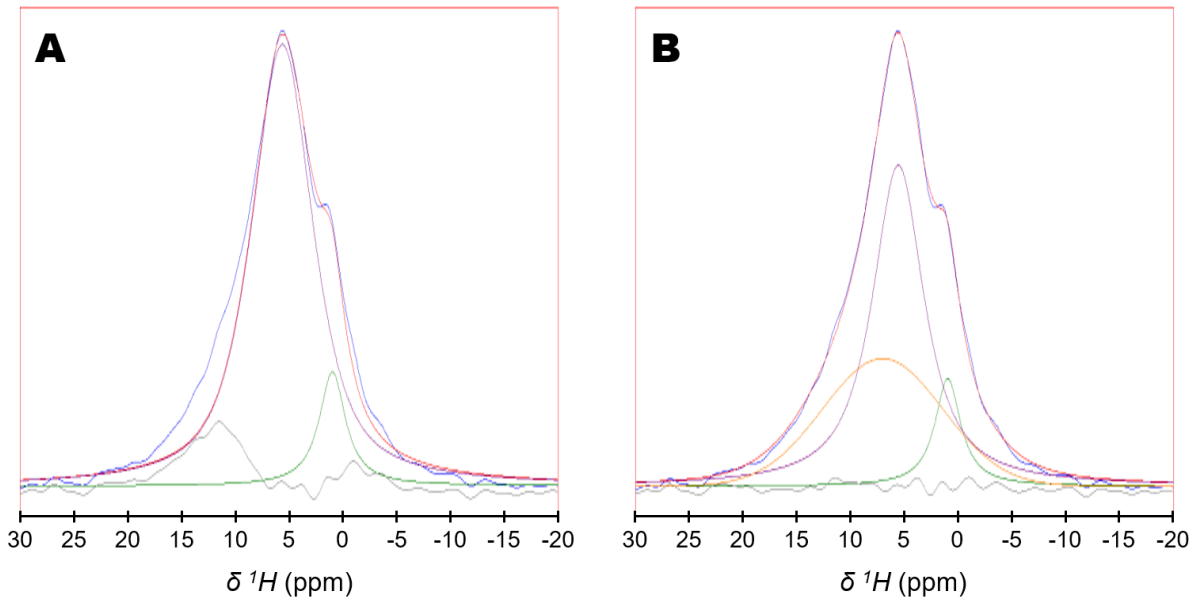

Figure S6. Rigid hydrogen-bearing ions/molecules present in the amorphous nanoparticles. (A) Normalized 1D $\{^{1}H\text{-}^{13}C\}^{1}H$ double cross polarization (CP) MAS ssNMR spectrum of the synthetic, Amorphous Calcium Magnesium Carbonate (ACMC) sample in dry conditions (**blue line –** shown in Fig. S5B); and its corresponding fitting (**red line**) using two peaks at $\delta(^{1}H)$ = 1.0 ppm (**green line**; FWHM = 2.9 ppm) and 5.6 ppm (**purple line**; FWHM = 6.8 ppm). **(B)** Normalized 1D $\{^{1}H\text{-}^{13}C\}^{1}H$ double cross polarization (CP) MAS ssNMR spectrum of ACMC in dry conditions (**blue line** - shown in Fig. S5B); and its corresponding fitting (**red line**) using three peaks at $\delta(^{1}H)$ = 1.0 ppm (**green line;** FWHM = 2.9 ppm), 5.6 ppm (**purple line;** FWHM = 5.8 ppm) and 7.0 ppm (**orange line**; FWHM = 13.1 ppm). The **gray lines** correspond to the residuals from the fittings.

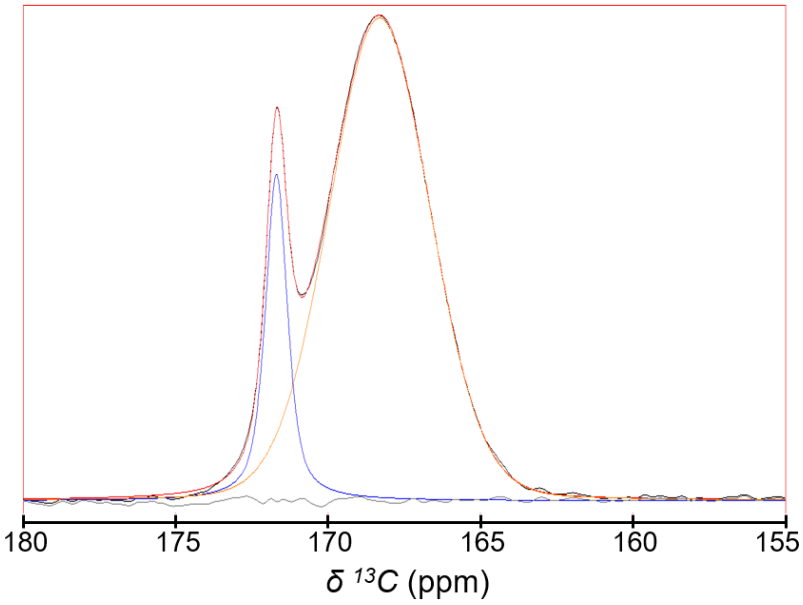

Figure S7. Evaluation of the conversion rate into monohydrocalcite. Quantitative ^{13}C single-pulse (SP) MAS ssNMR spectrum (recycling delay, RD = 600 s; number of scans, NS = 8; MAS frequency, ν_{MAS} = 8 kHz) of the synthetic, Amorphous Calcium Magnesium Carbonate (ACMC) sample soaked in deionized water and partially converted into monohydrocalcite (conversion rate, 15%) (**black line**), and its corresponding fitting (**red line**) using two peaks. The left peak drawn in **blue** [observable at $\delta(^{13}C)$ = 171.7 ppm; FWHM = 0.70 ppm - Lorentzian line shape] corresponds to the nascent crystalline environments in the form of monohydrocalcite; whereas the right peak drawn in **orange** [observable at $\delta(^{13}C)$ = 168.2 ppm; FWHM = 3.9 ppm - Gaussian line shape] corresponds to the starting amorphous environments. The **gray line** corresponds to the residuals from the fittings.

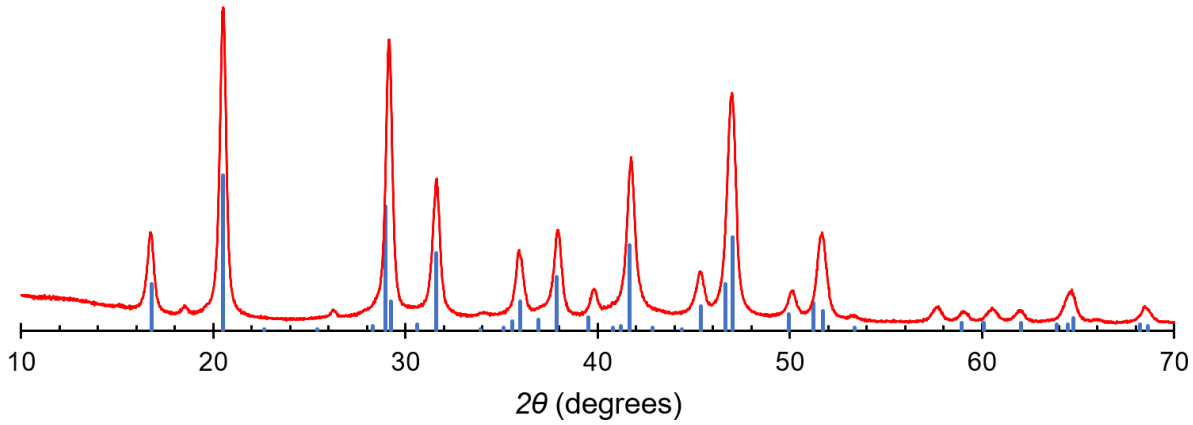

Figure S8. X-ray diffraction analysis of the monohydrocalcite sample prepared by a direct precipitation method. Powder X-Ray diffraction pattern of the synthetic, monohydrocalcite (MHC) sample in dry conditions (**solid red line**). Also shown is the PDF card of monohydrocalcite ($CaCO_3.H_2O$) in the ICDD database, number #029-0306 (**solid blue lines**).

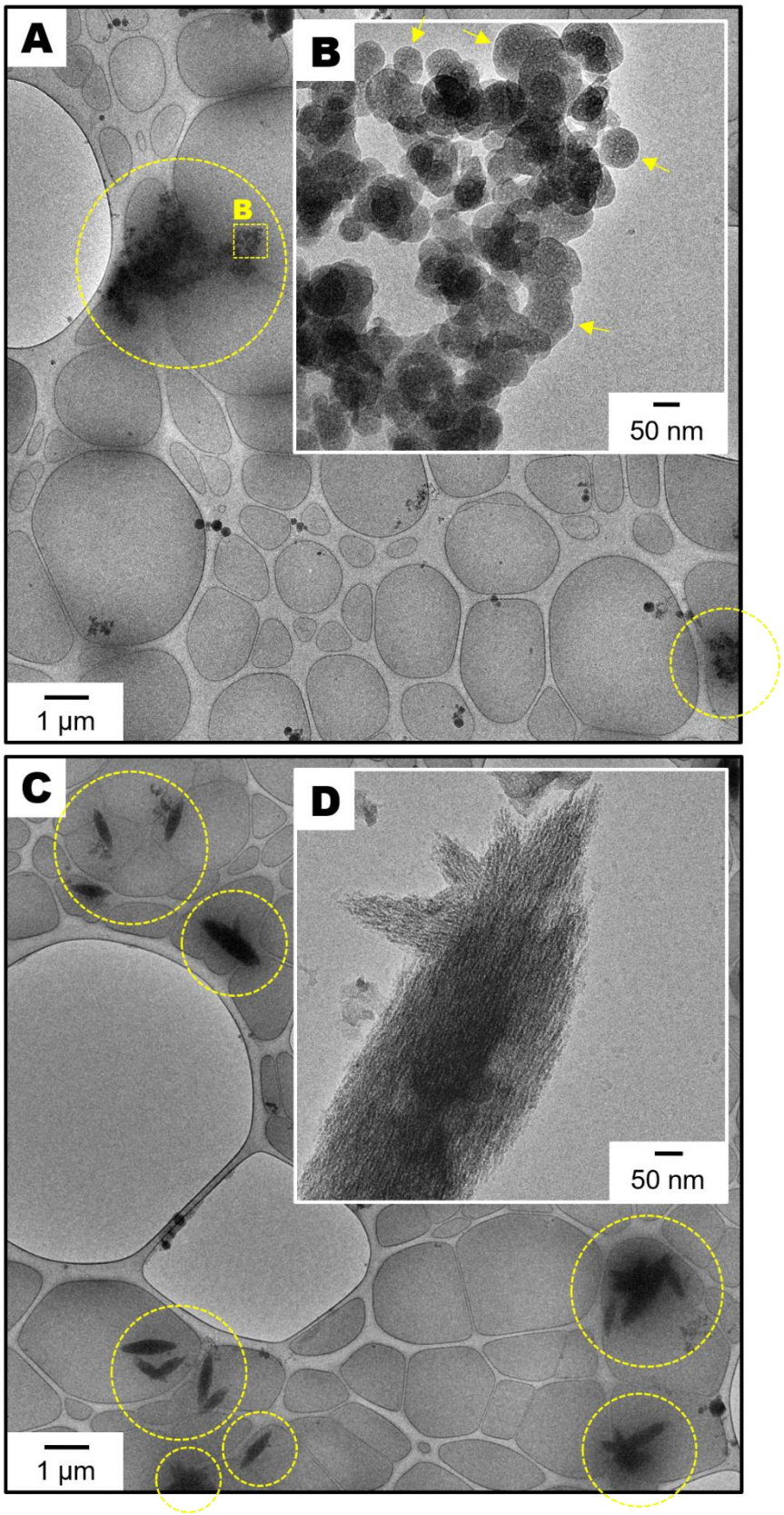

Figure S9. Observations of the starting amorphous nanoparticles and their resulting higher-order mineral structures following crystallization in water. (**A** and **B**) Representative cryogenic transmission electron microscopy (cryo-TEM) micrographs of the synthetic, Amorphous Calcium Magnesium Carbonate (ACMC) sample dispersed in deionized

water. (A) is a low magnification micrograph that displays the presence of aggregates of nanoparticles that are highlighted in yellow circles. (B) shows a magnification of the square region marked by the yellow dashed line drawn in (A); it reveals the morphological features of the amorphous nanoparticles that compose one of the aggregates shown in (A). (**C** and **D**) Representative SHIM micrographs of the higher-order mineral structures resulting from the crystallization of the synthetic ACMC sample soaked in deionized water in a 10 mL vial. These higher-order mineral structures are seen at low magnification in (C) where they are highlighted in yellow circles, and at high magnification in (D).

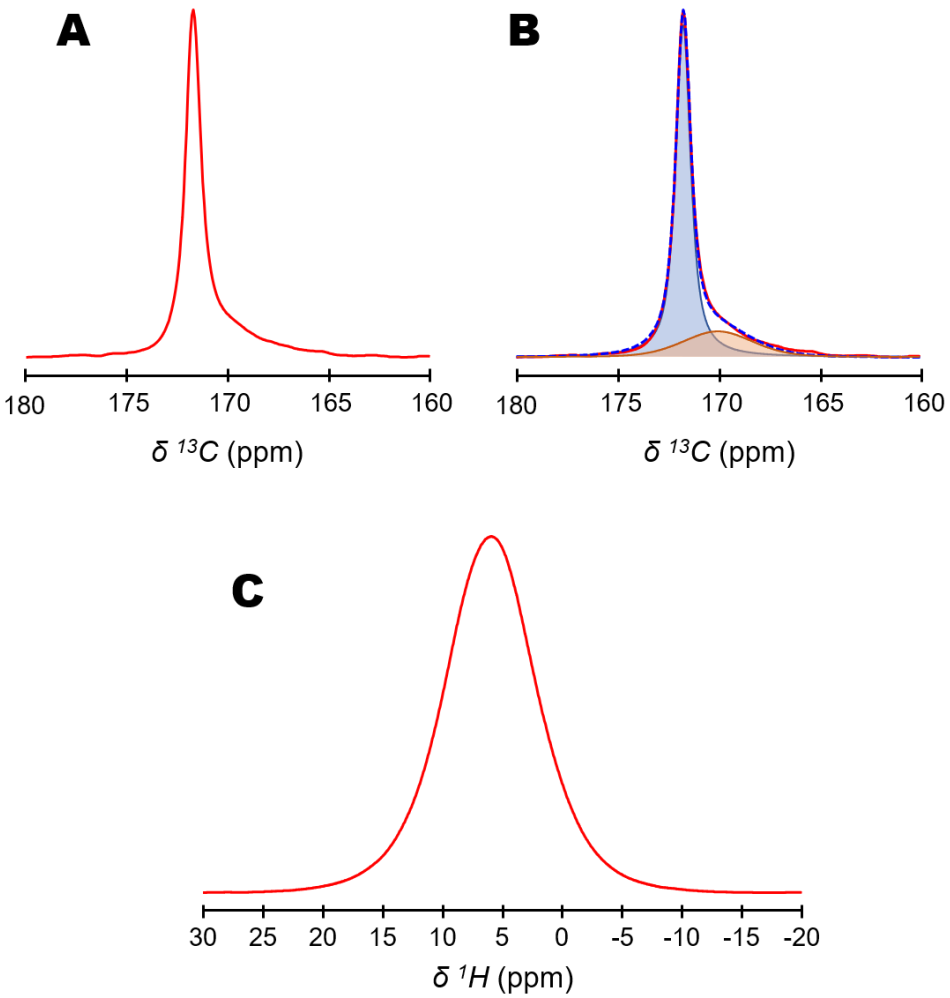

Figure S10. Carbon and Hydrogen environments of the synthetic monohydrocalcite sample. (**A**) 1D ^{13}C single-pulse (SP) MAS ssNMR spectrum (NS = 12; relaxation delay, RD = 600 s; MAS frequency, ν_{MAS} = 14 kHz) of the synthetic monohydrocalcite (MHC) sample in dry conditions. (**B**) 1D ^{13}C SP MAS ssNMR spectrum of the MHC sample shown in (A) (red solid line), and its corresponding fitting (blue dashed line) using two peaks. The left peak drawn in blue [observable at $\delta(^{13}C)$ = 171.7 ppm; FWHM = 0.70 ppm] corresponds to monohydrocalcite environments; whereas the right peak drawn in orange [observable at $\delta(^{13}C)$ = 169.5 ppm; FWHM = 3.8 ppm] corresponds to residual amorphous environments that were not converted into monohydrocalcite. The present fitting allows for determining the molar percentage of carbon ions present in monohydrocalcite and amorphous environments in the MHC sample, respectively about 80% and 20%. (**C**) 1D $\{^{1}H\text{-}^{13}C\}^{1}H$ double cross polarization (CP) MAS ssNMR spectrum (number of scans, NS = 2048; relaxation delay, RD = 2 s; contact time-1, t_{CP1} = 4 ms; contact time-2, t_{CP2} = 4 ms; ν_{MAS} = 14 kHz) of MHC in dry conditions.

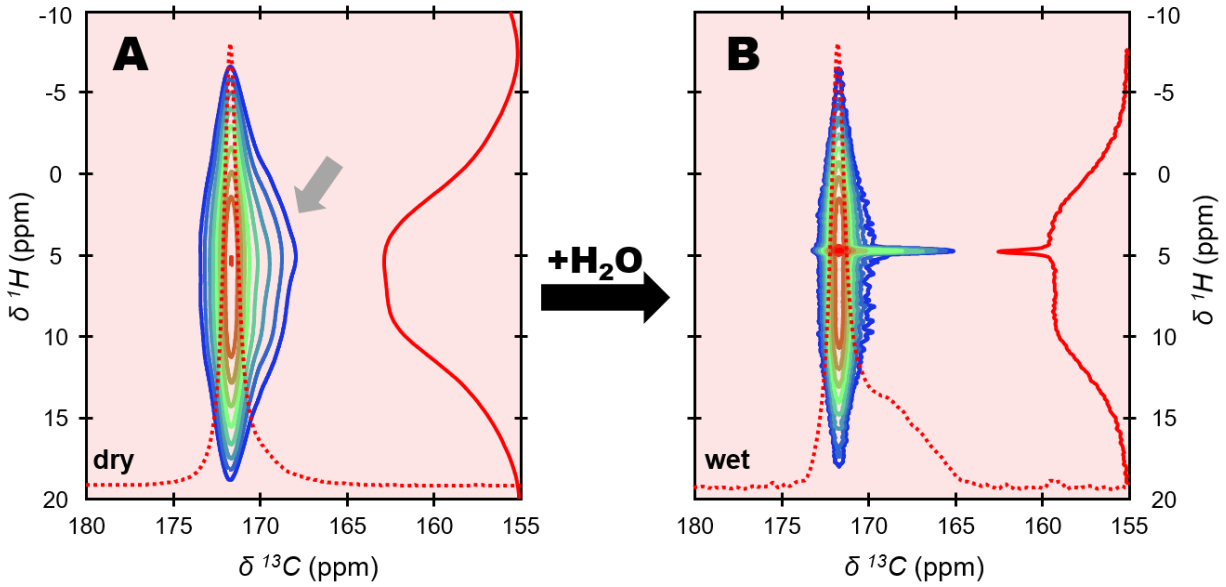

Figure S11. Spatial proximities among carbon-bearing ions and hydrogen-bearing ions/molecules in the particles of the monohydrocalcite sample. Contour plots of 2D $\{^{1}H\}^{13}C$ Heteronuclear Correlation (HetCor) MAS ssNMR spectra [contact time, t_{CP} = 4 ms; 32 (dry conditions) or 16 (wet conditions) scans in each 256 t1 increments; relaxation delay, RD = 1.5 s; MAS frequency, ν_{MAS} = 8 kHz] of the synthetic monohydrocalcite (MHC) sample in dry conditions (**A**) and soaked in deionized water (**B**). The signal intensity increases from blue to red. Also shown are the normalized, projections of the vertical, indirect ^{1}H dimensions (solid lines) and of the horizontal, direct ^{13}C dimensions (dotted lines) of these two 2D $\{^{1}H\}^{13}C$ HetCor MAS ssNMR spectra.

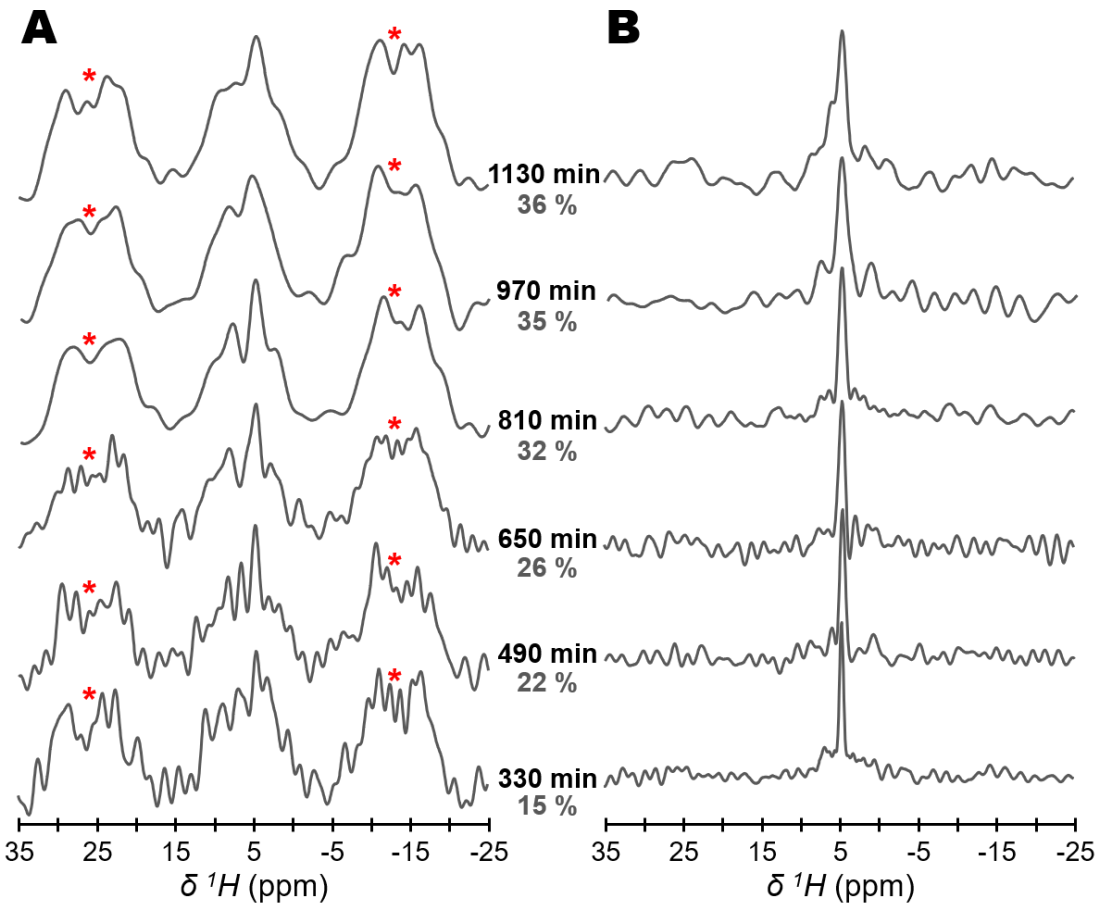

Figure S12. Evolution of the hydrogen environments while the amorphous nanoparticles are crystalizing in water. Shown are normalized, indirectly detected ^{1}H ssNMR spectra of the nascent crystalline environments in the form of monohydrocalcite (**A**); and of the starting amorphous environments (**B**) from the synthetic, Amorphous Calcium Magnesium Carbonate (ACMC) sample soaked in deionized water while crystallization progresses. These indirectly detected ^{1}H ssNMR spectra were all extracted from the different 2D {^{1}H}^{13}C Heteronuclear Correlation (HetCor) MAS ssNMR spectra shown in Fig. 5; and, correspond to ^{1}H slices taken at the monohydrocalcite (A) and ACMC (B) positions in the horizontal, direct ^{13}C dimensions. The different percentages are the conversion rate of ACMC into monohydrocalcite, whereas the different periods (given in min) correspond to the time during which the sample has been soaking in deionized water following the initial wetting step. It is worth mentioning that the ^{1}H slices taken at the ACMC position evolve over time: the resonance progressively become broader showing a fwhm of ≈ 0.6 ppm after 330 min (conversion rate, 15%) and of ≈ 1.3 ppm after 1130 min (conversion rate, 36%), corresponding to a linewidth increase of roughly 120%. This progressive broadening could reflect a change of dynamics during crystallization, namely a gradual decrease of the chemical exchange rate between hydrogens from the rigid ions/molecules present in the starting amorphous environments and those from the free water molecules. But this could also be due to a higher distribution of NMR chemical shifts (i.e., water molecules found in increasingly heterogeneous environments), along with bulk magnetic susceptibility effects as crystallization progresses. The red asterisks (*) denote intense spinning sidebands.

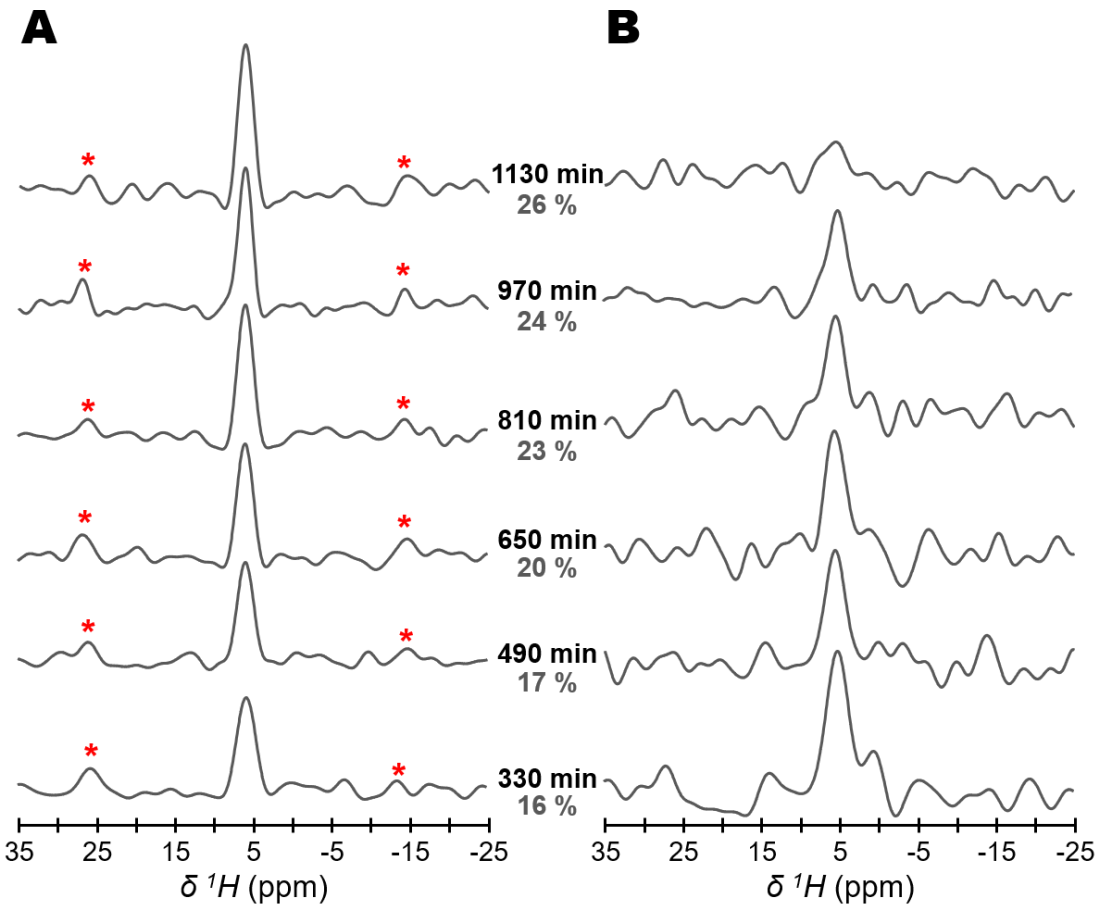

Figure S13. Evolution of the hydrogen environments while the amorphous nanoparticles are crystalizing in heavy water. Shown are non-normalized, indirectly detected ^{1}H ssNMR spectra of the nascent crystalline environments in the form of monohydrocalcite (**A**); and of the starting amorphous environments (**B**) from the synthetic, Amorphous Calcium Magnesium Carbonate (ACMC) sample soaked in heavy water (D_2O - 99.99 atom % D) while crystallization progresses. These indirectly detected ^{1}H ssNMR spectra were all extracted from the different 2D {^{1}H}^{13}C Heteronuclear Correlation (HetCor) MAS ssNMR spectra shown in Fig. 6; and, correspond to ^{1}H slices taken at the monohydrocalcite (A) and ACMC (B) positions in the horizontal, direct ^{13}C dimensions. The different percentages are the conversion rate of ACMC into monohydrocalcite, whereas the different periods (given in min) correspond to the time during which the sample has been soaking in heavy water following the initial wetting step. The red asterisks (*) denote weak spinning sidebands.

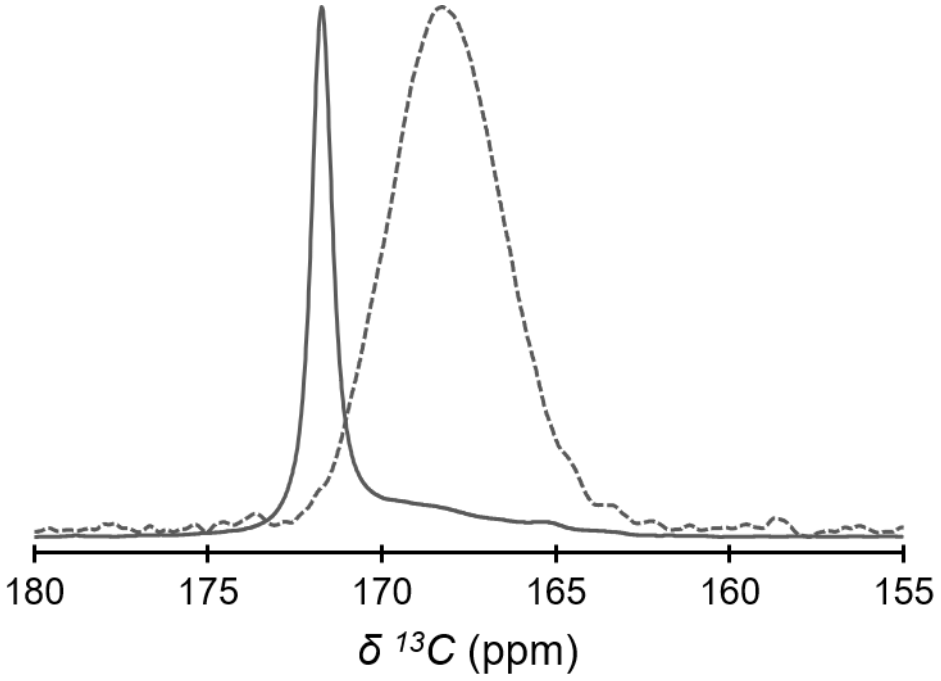

Figure S14. Carbon environments before and after crystallization. Normalized ^{13}C single-pulse (SP) MAS ssNMR spectra (recycling delay, RD = 600 s; number of scans, NS = 8; MAS frequency, ν_{MAS} = 8 kHz) of the synthetic, Amorphous Calcium Magnesium Carbonate (ACMC) sample in dry conditions (**dashed gray line**), and of ACMC converted into monohydrocalcite following its crystallization in deionized water in the MAS rotor for a period of approximately 2500 min (**solid gray line**).

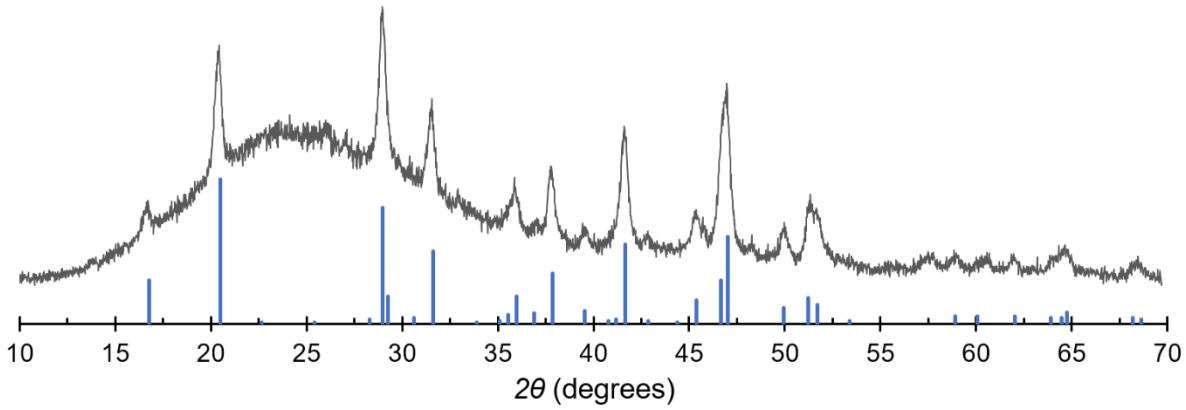

Figure S15. X-ray diffraction analysis of the synthetic amorphous nanoparticles following crystallization. Powder X-Ray diffraction pattern of the synthetic, Amorphous Calcium Magnesium Carbonate (ACMC) sample converted into monohydrocalcite following its crystallization in deionized water in the MAS rotor (**solid gray line**). Also shown is the PDF card of monohydrocalcite (MHC; $CaCO_3.H_2O$) in the ICDD database, number #029-0306 (**solid blue lines**).

References

(1) Nebel, H.; Epple, M. Continuous Preparation of Calcite, Aragonite and Vaterite, and of Magnesium-Substituted Amorphous Calcium Carbonate (Mg-ACC). *Z. Für Anorg. Allg. Chem.* **2008**, *634* (8), 1439–1443. https://doi.org/10.1002/zaac.200800134.

(2) Nishiyama, R.; Munemoto, T.; Fukushi, K. Formation Condition of Monohydrocalcite from CaCl2–MgCl2–Na2CO3 Solutions. *Geochim. Cosmochim. Acta* **2013**, *100*, 217–231. https://doi.org/10.1016/j.gca.2012.09.002.

(3) Schmidt, M. P.; Ilott, A. J.; Phillips, B. L.; Reeder, R. J. Structural Changes upon Dehydration of Amorphous Calcium Carbonate. *Cryst. Growth Des.* **2014**, *14* (3), 938–951. https://doi.org/10.1021/cg401073n.